

How can dugongs (*Dugong dugon*) travel along the water column at low energetic cost? A novel hypothesis

Jean-Pierre Lefebvre

IRD, UMR 250 - ENTROPIE, FRANCE, Université de la Réunion – Saint-Denis, Campus de Moufia, BAT S4A, 15 avenue Pierre Cassin, BP 7151, 97715 Saint-Denis, La Réunion, France

ARTICLE INFO

Keywords:

Dugong
Dugong dugon
 Surface envelope model
 Buoyancy
 Energetic cost

ABSTRACT

Dugongs (*Dugong dugon*) spend most of their lifetime either travelling between the sea surface and shallow seafloors where they forage seagrass beds or swimming just below the sea surface. Observations indicate that these movements are carried out with a very limited or even without swimming activity. We propose the novel hypothesis that dugongs travel along the water column at low energetic cost by taking advantage of the compression of their gas-filled organs by depth-varying water pressure. This hypothesis was formulated in terms of physics as the problem of the vertical displacement through a fluid of a body, which buoyancy is related to the hydrostatic pressure. In absence of the required field measurements to solve this problem, both the total volume and the compressible volume of dugongs were modelled and approximations for their weights found in the literature were used. We examined the cases of slightly positively buoyant bodies at the sea surface that becomes neutrally buoyant just below the surface. The predicted duration of free sinking was consistent with field measurements. The energetic expenditure required to travel back from the seafloor to the surface was assessed. We found that the depths where the dugongs forage the most frequently, corresponded to where the changes in buoyancy due to the hydrostatic pressure only, were moderate.

1. Introduction

Dugongs are listed as “Vulnerable to extinction” at a global scale by the International Union for Conservation of Nature (Marsh and Sobt-zick, 2019). As strict herbivores, they are bound to travel frequently between the sea surface and the seafloor in order to consume up to 40 kg wet weight of seagrass per day (Anderson and Birtles, 1978; Lanyon 1991). Evaluating their ability to adapt their foraging patterns to environmental changes is key for the conservation of this species (Amamoto et al., 2009; Mayor et al., 2009; Wirsing and Heithaus, 2012; Thums et al., 2013; Brakes and Dall, 2016; Tol et al., 2016; Bayliss et al., 2019; Mishra et al., 2021). Among the many issues left to be solved, this work focuses on the assessment of energetic cost of two phases of a dive; the descending phase and ascending phase. Our approach tackles this question from the physics perspective.

Little is known about how dugongs (*Dugong dugon* Müller 1776) travel along the water column with an apparent great economy of effort. The role played by buoyancy is key for addressing the motion of dugongs along the water column because the magnitude and direction of the buoyant force facilitate or hinder the vertical component of the movement. It has been hypothesized that the bone density of sirenians

evolved over a long period to adapt their buoyancy toward a quasi-neutral buoyancy.

This quasi-neutral buoyancy is sometimes assumed to be actively modified within the short duration of diving cycles, by an action on the elongated and horizontally orientated lungs (Pabst et al., 1999). The changeable volume is sometimes thought to consist of intestinal gas; the buoyancy being affected by compression by abdominal muscles of by expelling methane (Rommel and Reynolds 2000). Marshall et al. (2022) did not attributed the overall control of movements to changes on slightly negative buoyancy of sirenians but to the action of diaphragm on lungs, solely affecting their horizontal trim in the water.

Field reports indicate that dugongs spend more than 72% of their lifetime within depths less than 3 m and 53%, foraging shallow seagrass beds deeper than 1.5 m and occasionally reaching depth of about 20 m, the deepest dives reported being of about 40 m (Marsh and Saalfeld, 1989; Chilvers et al., 2004; Sheppard et al., 2006). They have been observed floating motionlessly near the surface at a depth of less than 3 m (D'Souza and Patankar, 2009) and resting or crawling on the seafloor even at shallow depth (Hodgson, 2004). These observations imply that dugong buoyancy changes from quasi-neutral just below the sea surface to slightly negative at shallow depths.

E-mail address: jean-pierre.lefebvre@ird.fr.

<https://doi.org/10.1016/j.ecolmodel.2023.110505>

Received 24 April 2023; Received in revised form 11 September 2023; Accepted 12 September 2023

Available online 17 September 2023

0304-3800/© 2023 The Author. Published by Elsevier B.V. This is an open access article under the CC BY-NC-ND license (<http://creativecommons.org/licenses/by-nc-nd/4.0/>).

If it is documented that some cetaceans can alter the shape of their thorax by muscular constriction (Cotten et al., 2008), the physiological features needed to exert this control were not found for dugongs (Domning and De Buffénil, 1991). In consequence, an external force must be responsible for this change in volume. Chest-wall collapse with water pressure is well documented for breath-hold diving mammals (e.g. Brown and Butler, 2000). For species that can swim energetically over long distances, such as dolphins (Skrovan et al., 1999), whales (Nowacek et al., 2001; Miller et al., 2004) and seals (Aoki et al., 2011), this change in buoyancy merely provides an alleviation of the effort during sequences of glide (Trassinelli, 2016). Dugongs differ from these species by a general sluggishness and an inability to sustain effort more than few minutes (Marsh et al., 1978; Anderson, 1981). Moreover, because of their strict herbivorous diet, they do not need to control their trajectories, as strictly as species that chase their preys.

We propose a novel hypothesis: dugongs merely take advantage of the slight change in buoyancy due to the compression of their gas-filled organs by the depth-changing water pressure. To fit the above-mentioned observations, the buoyancy must become neutral at a depth of less than 3 m under the sea surface which means that it must be slightly positive at the sea surface and becomes slightly negative only below that neutral buoyancy depth.

The data required to quantify the change in buoyancy, and hence to validate any hypothesis on how dugongs manage to change their depth almost effortlessly being unavailable, we modelled our assumption in a physics perspective and showed that the obtained results felt within the range of available field observations and measurements, considering a conservative error margin.

2. Methods

In a physics perspective, our hypothesis is formulated as the quantification of the motion of a dugong along the water column, with its buoyancy changing due only to the action of the hydrostatic component of the water pressure on its gas-filled organs. With Newton's second law of motion, the change in velocity vector U ($m.s^{-1}$) of a body is related to its mass W (kg) and to the sum of forces F (N) acting upon it:

$$W \frac{\partial \vec{U}}{\partial t} = \sum \vec{F} \quad (1)$$

The weight of the dugong is assumed to remain unchanged during a dive. Four main forces act upon the body moving through a fluid: the buoyancy force (F_B), the drag force (F_D), thrust force (F_T), and the lift force, which can be neglected here, because of the low velocities that dugongs attain. Considering only the vertical components in Eq. (1), the acceleration at any depth z is:

$$W \frac{\partial U(z)}{\partial t} = F_D(z) + F_T(z) + F_B(z) \quad (2)$$

The intensity of the drag force generated by the motion of a body at a velocity U is expressed as (Lauder and Tytell, 2006):

$$F_D(z) = -C_D \frac{\rho_w SA}{2} U(z)^2 \quad (3)$$

where SA (m^2) is the total surface area of the object and C_D , an adimensional drag coefficient depending of the shape of the body. The sea water density ρ_w is taken as 1021 kg.m^{-3} .

The thrust force of swimming marine mammals can be expressed as a function of the propulsive area of its fluke (PA_{fluke} , m^2) and of the amplitude and frequency of its undulation (f_{tail} , Hz) (Lauder and Tytell, 2006; Kojaszewski and Fish, 2007; Fish et al., 2008; Trassinelli, 2016; Jung, 2021).

The buoyancy force (F_B , N) is the result of the attraction force applying on a body of apparent weight W_a (kg). Expressing the apparent weight at any depth z , the buoyancy force is:

$$\vec{F}_B(z) = g W_a = g(W - \rho_w V_{tot}^z) \quad (4)$$

g is acceleration due to gravity and V_{tot}^z (m^3) represents the total volume of a dugong at depth z .

Neglecting the compressibility of the dense tissues, this volume change between two depths z_1 and z_2 is related to the compression of a volume of gas only:

$$\Delta V_{tot}^{z_1 \rightarrow z_2} = V_{tot}^{z_2} - V_{tot}^{z_1} = V_{gas}^{z_2} - V_{gas}^{z_1} \quad (5)$$

We assume the quantity of gas remains constant during a dive. Hereafter, the superscript indicates the depth under the still water level (SWL), where the variable is defined.

Introducing the assumption that the compression of the gas is due to the hydrostatic component of the water pressure, with Boyle's law, the compression of a gas at any depth z , that occupies a volume V_{gas}^0 (i.e. the volume occupied by the quantity of gas under the atmospheric pressure at sea level $P_{atm} = 101,325 \text{ Pa}$) occupies a volume:

$$V_{gas}^z = \frac{P_{atm}}{P_h(z)} V_{gas}^0 \quad (6)$$

where $P_h(z)$ (Pa) is the hydrostatic component of the water pressure:

$$P_h(z) = \rho_w g z + P_{atm} \quad (7)$$

The actual compressible air storage compliance being documented for few marine mammals only (e.g. Fahlman et al., 2011; Moore et al., 2014) but not for sirenians, the elasticity of the chest wall is neglected in Eq. (6).

According to our hypothesis, the buoyancy of a dugong becomes neutral for a depth z_n (m) in the vicinity of the SWL. The total volume at the neutral buoyancy depth z_n is:

$$V_{tot}^{z_n} = \frac{W}{\rho_w} \quad (8)$$

From Eqs. (4)-(6), we obtain a relationship between on one hand, the weight and the total and gas volume at SWL of a dugong, and on the other hand, the depth where its buoyancy becomes neutral:

$$W = \rho_w \left(V_{tot}^0 - \frac{z_n}{z_n + z_{atm}} V_{gas}^0 \right) \quad (9)$$

where z_{atm} (m) is the conversion as an offset of the contribution of atmospheric pressure at sea surface: $z_{atm} = \frac{P_{atm}}{\rho_w g}$.

Five length to weight relationships (LWR) for dugongs found in the literature were used in this study: four were obtained from cadavers (Nair et al. 1975; Spain and Heinsohn, 1975; Adulyanukosol et al., 2009; Cherdukjai et al., 2020) and one from living wild dugongs (Lanyon et al., 2010). When the raw data were indicated, the LWR was rewritten as a power law.

Since neither the total nor the gas volume of a dugong has been measured, they were approximated by two sub-models: a surface envelope model (SEM), and a gas sub-model, respectively.

Even so, all the independent variables for these two sub-models are not documented. For the missing ones, their ranges were determined empirically, based on "realistic" and yet, conservative assumptions in order to prevent a significant impact on the results. All the combinations of all the possible values for all independent variables were tested and those which are not a solution of Eq. (9) are rejected.

This work was entirely developed with Matlab R2019a (The Mathworks Inc.). All fitting of functions to data used the ordinary least square fitting method, so we assumed Gaussian errors in all statistical analyses.

2.1. Surface envelope sub-model (SEM)

The SEM approximates the total volume (V_{tot} , m^3) as the sum of the

volumes of the snout, the head, the trunk, the two flippers and the fluke:

$$V_{tot} = V_{snout} + V_{head} + V_{trunk} + V_{flippers} + V_{fluke} \quad (10)$$

The flippers and fluke shapes are taken as planar. Their modelling is detailed in the Appendix 1. The snout, head and trunk are modelled as surfaces of revolution.

2.1.1. Trunk

The trunk is defined as the segment of the body, comprised between the back of the skull to the apex of the notch in the tail fluke, excluding the flippers and the fluke. Following Domning and De Buffr enil (1991), the contour shapes of transverse sections along the longitudinal axis are considered as approximately elliptic. Due to the asymmetry between the belly and the back, these contours are modelled as two semi-ellipses (Fig. 1) and are expressed by three parameters: the scaling radius R (m), equal to half the minor axis of the upper semi-ellipse, and two adimensional factors: one in the frontal plane, defined as the ratio between half the major axis of a semi-ellipse and the scaling radius (α), and the other in the sagittal plane as the ratio between half the minor axis of the lower semi-ellipse and the scaling radius (β).

The variation of the girth along the longitudinal axis is modelled as a foil:

$$G_{BL}(\ell) = a_0(BL)\ell^{0.5} + a_1(BL)_{BL}\ell + a_2(BL)\ell^2 + a_3(BL)\ell^3 + a_5(BL)\ell^4 \quad (11)$$

where G_{BL} (m) is the girth of a dugong of body length BL measured at the distance ℓ (m) along the longitudinal axis, the origin of this axis being fixed at the tip of the snout.

The coefficients a_0 to a_5 in Eq. (11) are determined for each BL , by fitting the locations and values of six girths obtained with allometric equations (Spain and Heinsohn, 1975): at the anterior and posterior neck, umbilicus, anus, base of the tail fluke and with an additional null girth at the distance BL . Since size allometry was determined from out of water animals, the SEM is considered as the surface envelope of a body at SWL (i.e. at the atmospheric pressure P_{atm}).

The scaling radius R_{BL} (m) at the distance ℓ is related to the expression of the girth in Eq. (11) as:

$$R_{BL}(\ell, \alpha, \beta) = \frac{2}{\pi} (K_{\alpha,1} + K_{\alpha,\beta})^{-1} G_{BL}(\ell) \quad (12)$$

where $K_{\alpha,\beta}$ is an adimensional function obtained from Ramanujan's approximation for the perimeter of an ellipse (Villarino, 2006):

$$K_{\alpha,\beta} = 3(\alpha + \beta) - \sqrt{(3\alpha + \beta)(\alpha + 3\beta)} \quad (13)$$

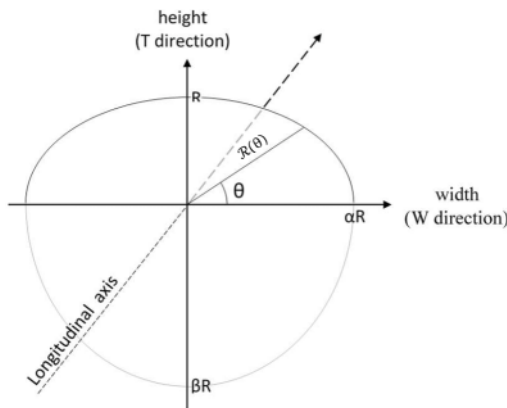


Fig. 1. Contour of a transverse section within the trunk segment modelled as two semi-ellipses defined by the scaling radius (R , m) and two adimensional semi-ellipse shape factors (α and β). The contour equation of both semi-ellipses can be conveniently expressed in a polar coordinate system ($\mathcal{R}(\theta)$).

Assuming a contour shape strongly correlated with the shape of the rib cage, the two semi-ellipse shape factors α and β are taken as constant along the longitudinal axis within the trunk.

An approximation for the volume of the trunk segment comprised between the base of the skull and the anus is calculated. It is identified as the volume for the neck, abdomen and thorax (V_{nta} , m³) and is used in the gas sub-model (see below).

2.1.2. Snout

The snout is modelled as a semi-oblate ellipsoid (Marsh, 1989). Its volume and surface area are calculated with the corresponding canonical equations.

2.1.3. Head

The shape of the head is modelled as an irregular truncated cone with a circular section in the transverse plan at the snout to elliptic section in the transverse plan at the neck (i.e. α and β dependent of ℓ). The volume of the head can be expressed analytically but not its surface area which is approximated numerically. The detail of the calculations of surface area and volume of the five segments of the SEM can be found in Appendix 2.

2.1.4. Flattening (f) and fineness ratio (FR)

The two ellipse shape factors α and β constitute with BL (and marginally the sex of the animal), the independent variables of the SEM (Eqs. (10)-(12)). Contrarily to BL , which range is easily assessable, fixing a realistic range for α and β is less intuitive. For this reason, we introduce two more assessable shape parameters: the flattening and the fineness ratio.

The adimensional flattening coefficient (f) quantifies how far from circular the contour of an ellipse is (f varying from 0 for a circular contour and 1 for a flat one):

$$f = 1 - \frac{\text{length}_{\text{minor axis}}}{\text{length}_{\text{major axis}}} \quad (14)$$

This concept is adapted for a contour constituted of two semi-ellipses. Two cases have to be distinguished: either the contour in the transverse section of the trunk (TST) is taller than wide ($2\alpha \leq \beta + 1$) or wider than tall ($2\alpha > \beta + 1$). These two cases are termed 'T-shaped' and 'W-shaped', respectively. The adimensional flattening coefficients for the two TST are:

$$T\text{-shaped} : f = 1 - \frac{2\alpha}{\beta + 1} \quad (15.1)$$

$$W\text{-shaped} : f = 1 - \frac{\beta + 1}{2\alpha} \quad (15.2)$$

Since this parameter is not reported in the literature, the realistic maximal value for the flattening is fixed from examinations of pictures and videos as $f_{\text{max}} = 0.25$.

The fineness ratio (FR) is the only shape parameter documented for dugongs (Fish, 1993). This adimensional parameter is defined as the ratio of the body length to the maximum thickness (T_{max} , m) in the transverse planes:

$$FR = \frac{BL}{T_{\text{max}}} \quad (16)$$

This parameter indicates whether a body shape is likely to generate a significant drag force when moving through a fluid. Fish (1993) evaluated FR ranging between 4.0 and 4.5 for dugong which corresponds to the optimum value yielding a minimum drag force for the maximum volume. It indicates that the body of dugong is streamlined and supports the choice to model the longitudinal shape of the trunk as a foil (Eq. (11)). As for f , FR depends of the dugong TST:

$$T\text{-shaped} : FR = \frac{BL}{(\beta + 1)R_{\text{max}}} \quad (17.1)$$

$$W - \text{shaped} : FR = \frac{BL}{2\alpha R_{max}} \quad (17.2)$$

with R_{max} , the maximum value for $R_{BL}(l, \alpha, \beta)$ in Eq. (12).

2.2. Gas sub-model

Two gases are considered in this sub-model: the air and the methane:

$$V_{gas} = V_{air} + V_{methane} \quad (18)$$

It is beyond the scope of this paper to model a physiological functioning of the respiratory or digestive tracts of a dugong. The aim of the gas sub-model is to provide all possible values for the volume of gas (V_{gas} , m^3) based on combinations of independent variables restricted to their realistic ranges.

We introduce three adimensional factors: φ_{lungs} , φ_{air} and $\varphi_{methane}$, corresponding to the ratio between the volume of the lungs and of the neck, abdomen and thorax segment, between the volume of air and of the lungs, and between the volume of methane and of small and large intestine, respectively, at sea surface.

Considering that most of the organs containing a significant volume of air (e.g. lungs, windpipe) are located between the base of the skull and the anus, we relate the approximation of the lungs volume at SWL (V_{lungs}^0 , m^3) to V_{nta} :

$$V_{lungs}^0 = \varphi_{lungs} V_{nta}^0 \quad (19)$$

The air volume at sea surface (V_{air}^0 , m^3) is expressed in function of the lungs volume:

$$V_{air}^0 = \varphi_{air} V_{lungs}^0 = \varphi_{air} \varphi_{lungs} V_{nta}^0 \quad (20)$$

Since air can be stored outside the lungs (e.g. in the windpipe), φ_{air} can exceed 1.

Methane is the main by-product of fermentation by intestinal bacteria of ingested seagrass. At SWL, the volume of methane ($V_{methane}^0$, m^3) is related the volume of the small and large intestine ($V_{intestines}^0$, m^3) as:

$$V_{methane}^0 = \varphi_{methane} V_{intestines}^0 \quad (21)$$

$V_{intestines}^0$ obtained by taking the shape of the intestines as cylindrical. Their lengths are obtained from allometric and their mean diameter taken equal to 4.5 and 7 cm, for the small and large intestine, respectively.

The three adimensional factors: φ_{lungs} , φ_{air} and $\varphi_{methane}$ constitutes the independent variables of the gas-sub model.

2.3. Validation of the hypothesis

Due to bias in the allometry and LWR, it is necessary to assess the modelling error, to select the less flawed data and correct them. Finally, the validity of our hypothesis is checked by verifying that some of the selected data satisfy Eq. (9).

2.3.1. Mitigation of the uncertainty on the weight and neutral buoyancy depth

From a modelling perspective, the weight approximated with LWR (W_{BL}) is used as an *a priori* value and the weight obtained with Eq. (9) correspond to a *posteriori* approximation of the weight. These two values may differ due to the modelling errors. To circumvent this discrepancy, the supposedly most accurate LWR (i.e. Lanyon et al.'s only LWR based on living wild animals) can be selected. But since the modelling error stems not necessarily from a simple addition of all sources of errors, instead, we choose to mitigate the specific modelling error attached to each LWR. We define an adimensional rescaling parameter (λ) based on the ratio of the *a priori* and *a posteriori* value of weight:

$$\lambda = \left(\frac{W_{BL}}{W} \right)^{1/3} \quad (22)$$

Assuming that the intrinsic error of the model affects linearly all the output variables, all modelled volumes are corrected as $\lambda^3 V$, all modelled areas, as $\lambda^2 A$ and all modelled lengths, as λL . The corrected V_{tot} and V_{gas} , ensure W in Eq. (9) and W_{BL} to be equal. Nevertheless, assuming that the impact of λ on the model is likely to artificially constrain the solution for λ further from 1, all the sets of solutions of associated to $|1 - \lambda| > 0.05$ are rejected.

Similarly, after inserting the corrected values of $\Delta V_{tot}^{0 \rightarrow \tilde{z}_n}$ and V_{gas}^0 in Eqs. (8) and (9), the corrected *a posteriori* neutral buoyancy depth (\tilde{z}_n , m) is:

$$\tilde{z}_n = \frac{z_{atm} \Delta V_{tot}^{0 \rightarrow \tilde{z}_n}}{\lambda^3 V_{gas}^0 - \Delta V_{tot}^{0 \rightarrow \tilde{z}_n}} \quad (23)$$

Where $\Delta V_{tot}^{0 \rightarrow \tilde{z}_n}$ (m^3) is the corrected loss of total volume between the surface and the neutral buoyancy depth z_n :

$$\Delta V_{tot}^{0 \rightarrow \tilde{z}_n} = \lambda^3 V_{tot}^0 - \frac{W}{\rho_w} \quad (24)$$

We choose to determine the value for $\varphi_{methane}$ that minimizes discrepancy between the *a priori* value for z_n and \tilde{z}_n . This value is obtained with the Nelder-Mead's method:

$$\varphi_{methane}^{opti} \Big|_{\tilde{z}_n \rightarrow z_n} = \frac{z_{atm} + \tilde{z}_n}{\tilde{z}_n V_{intestines}^0} \Delta V_{tot}^{0 \rightarrow \tilde{z}_n} - \varphi_{air} \frac{V_{lungs}^0}{V_{intestines}^0} \quad (25)$$

This optimization serves only the purpose to refine the overall modelled volume of gas that ensures the convergence of the *a priori* and *a posteriori* value for z_n but does not suggest any relation between the volume of air and methane.

The structure of the model is schematized on Fig. 2.

2.4. Parametric equations

As already explained, the formulation of our hypothesis in terms of physics results in Eq. (2) that is defined with five parameters V_{tot}^0 , V_{gas}^0 , PA_{fluke} , SA , $PA_{flippers}$. The selected values of these parameters satisfy Eq. (9). We produce a parametric equation for each of these parameters which allows to approximate their values as a result of a simple function of a small number of independent variables, and hence, without running the model.

This selection of variables is based on the calculation of Pearson Correlation Coefficient (PCC) between the values for each of the seven parameters and all independent variable of the model.

Although the type of each of these functions is *a priori* unknown, some of their properties can be inferred. As the body length of a dugong gradually increases with ageing, its volumes and surface areas are likely to increase steadily also. In other words, the five parametric equations must be smooth continuously differentiable functions of BL. It is also likely that the growth rate diminishes with ageing, and hence, the derivate of these parametric equations with respect to BL must decrease with increasing BL. Moreover, although not identical, the growth of the segments of the dugong must not be independent of each other.

The expressions of all parametric equations are presented in Appendix 3. The parametric equations for two more parameters affecting the gas volume at SWL: $V_{intestines}^0$ and V_{lungs}^0 are also provided.

3. Results

About $1.42 \cdot 10^{11}$ combinations of values for all independent variables spanning over their «realistic» ranges were tested. After restriction procedures, 427,392 combinations of values that satisfy Eq. (9) are

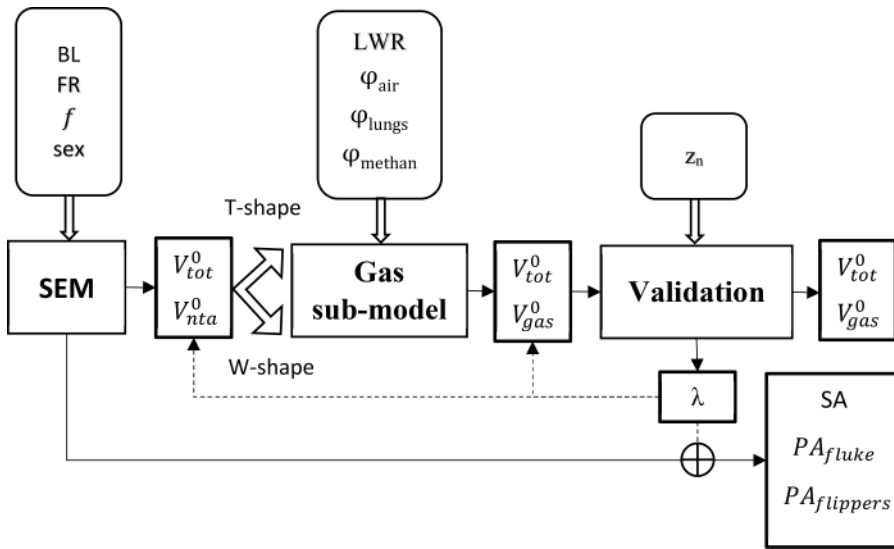


Fig. 2. Schematic representation of the model. From left to right, the surface envelope sub-model (SEM) estimates the total volume (V_{tot} , m^3), the segment comprising the gas-filled organs (V_{nta} , m^3) at sea level, the total surface area (SA, m^2) and the propulsive area of the flukes (PA_{flukes} , m^2) and of the two flippers ($PA_{flippers}$, m^2), for all combinations of body length (BL, m) and sex, and two adimensional shape factors: the fineness ratio (FR) and the flattening (f). Each calculated set of surfaces and volumes belongs to one of the two categories: either the contour in a transverse section of the trunk is taller than wide (T-shape) or wider than tall (W-shape). Next, the volumes of gas at sea surface corresponding to all the calculated volumes, and for all combinations of the three adimensional gas ratio factors: ratio of lungs volume to V_{nta} (ϕ_{lungs}) ratio of air volume to (ϕ_{air}) and ratio volume of methane on intestines ($\phi_{methane}$), and for the five implemented length to weight relationships (LWR) are defined. In the last part, the modelling errors are assessed for each sets of modelled values. The sets associated with the less significant error (λ) are corrected accordingly. Finally, the validity of our hypothesis (i.e. neutral buoyancy attained at a given depth z_n) is tested for all the remaining sets of parameters and all the possible values

for z_n .

selected. The «realistic» ranges for each independent variable are presented in Table 1.

3.1. Sensibility to the constraints in the gas sub-model

The unique measurement available indicates that the volume of the lungs of a dugong weighting 300 kg is approximately $0.045 m^3$ (Tenney and Remmers, 1963). The modelled results indicate that, at the sea surface, the lungs of a dugong weighting 300 kg occupy between 17 and 18% of its neck-thorax/abdomen segment (Table 2). The error between the modelled and measured lungs volume depends only slightly on LWR, TST and sex and not significantly of FR, f , z_n , ϕ_{air} and $\phi_{methane}$.

The ratio between the volume occupied by the lungs and the volume of the neck-thorax/abdomen probably decreases with increasing BL because the volume of the abdomen is likely to increase faster with ageing than the volume of the thorax constrained by the ribcage. However, in absence of measurements of the lungs volume for dugongs of various weight or body length, this trend cannot be ascertained. The results presented in Table 2 are taken as independent of the weight and hence of the body length. They are considered as an average value ($\phi_{lungs}^{average}$) for any BL ranging between 1.8 and 3.0 m.

3.2. Sensibility to the shape constraints in the SEM

The relationship between the longitudinal shape factor (fineness

Table 1

Ranges of each independent variable of the problem. Since dugong are always fully immersed, the lower bound for neutral buoyancy depth is set to half of the maximum thickness in the sagittal plane of the given dugong (see Fig. 1 and Eq. (16)). The abbreviation used in the text are indicated and the units of the parameters are reported in the second and fourth column, respectively.

Parameter	Abbreviation	Range	Unit
Body length	BL	1.8 – 3.0	m
Fineness ratio	FR	3.9 – 4.8	–
Flattening	f	0.0– 0.25	–
Neutral buoyancy depth	z_n	0.5 T_{max} – 3.0	m
Volume ratio air to lungs	ϕ_{air}	1.0 – 1.25	–
Volume ratio lungs to neck-thorax/abdomen segment	ϕ_{lungs}	0.1 – 0.25	–
Volume ration methane to intestines	$\phi_{methane}$	0.0 – 0.25	–

Table 2

Volume ratio of lungs to neck-thorax/abdomen (ϕ_{lungs}) that leads to a volume of $0.045 m^3$ for a dugong weighting 300 kg. These values are calculated for each length-weight relationship (left column) and sex, averaged over the restricted sets of solutions corresponding to the case of a transverse section of the trunk (TST) taller than wide (T-shaped) and wider than tall (W-shaped).

LWR	T-shaped		W-shaped	
	Male	female	male	female
Adulyanukosol et al.	0.172	0.177	0.174	0.180
Cherdsukjai et al.	0.174	0.177	0.173	0.177
Lanyon et al.	0.178	0.185	0.179	0.185
Nair et al.	0.185	0.180	0.185	0.179
Spain and Heinsohn	0.173	0.178	0.173	0.180

ratio, FR) and transverse shape factor (flattening, f) strongly depends of the TST. For the T-shaped case, FR never exceeds 4.5, as reported in Fish (1993). The flattening (f) decreases steadily to 0 (i.e. to circular TST) with increasing FR. The trend is opposite for the W-shaped case. The fineness ratio is always greater than 4.3 and TST becomes less circular (i.e. increasing flattening) with increasing FR (Fig. 3). The relationships between FR and f is independent of the selected LWR and sex.

3.3. Impact of the length to weight relationships (LWR) on the modelling error

As explained earlier, the model is based on allometry for the SEM and LWR for the gas sub-model. However, the resulting modelling error is not necessarily a simple addition of the errors related to these two sources. The model includes two procedure to assess and mitigate the modelling error: one is based on the adimensional rescaling parameter λ (Eq. (22)), and the other on the correction of the modelled gas volume at sea surface in the parametric equation for V_{gas}^0 (see Appendix 3). The results of these two procedures are examined below.

3.4. Adimensional rescaling parameter λ

The mean and standard deviation of the adimensional rescaling parameter λ serve as estimator for the contribution of each LWR to the total error of estimation. Recalling that the subset of solutions was restricted to those meeting the condition $|1 - \lambda| \leq 0.05$, we observe that

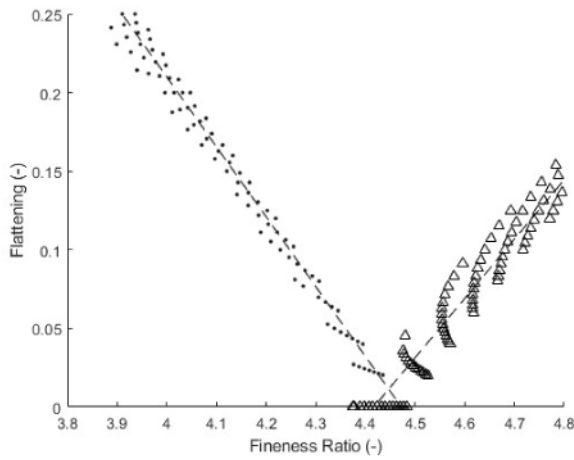


Fig. 3. Relationship between the fineness ratio (FR) and the flattening (f): The modelled relationship between FR and f inserted in the model is plotted with the dashed lines. The \bullet represent the individuals with transverse section of the trunk (TST) taller than wide (T-shaped) and the Δ , with TST wider than tall (W-shaped). The example presented here is calculated for a male dugong with a body length of 2.6 m. Its weight is approximated with the Spain and Heinsohn's length-weight relationship. φ_{luggs} is set to its average value (see Table 2).

the averaged values of λ are consistently greater to 1. This indicates that the bias of the model before corrections described in the paragraph ‘Mitigation the uncertainty on the weight and neutral buoyancy depth’, tends to slightly underestimate V_{tot} and V_{gas} of between 1.2 and 2.4%. This is consistent with the bias of allometry due to a possible loss of fluid and dehydration of the cadavers as discussed in Spain and Heinsohn (1975).

The error decreases with increasing BL for all LWR (not shown). The standard deviation of λ provides a good indicator for how consistently the predicted weight by the theoretical buoyancy-based weight is close of the approximated weight by LWR (Table 3). However, since this indicator is evaluated prior any mitigation of the modelling error, it cannot be used as an indicator for the impact of each LWR on the final results. Lanyon et al. (2010) LWR always resulted in the lowest standard deviation of λ for every tested case. However, the standard deviation of λ could not be considered as significantly high for any LWR. Unsurprisingly, no significant dependence to sex was found. Only a limited number of allometry equations were sex dependent in Spain and Heinsohn (1975) and no LWR but Nair et al.'s (1975).

3.5. Parametric equation for V_{gas}^0

The two fitting coefficients r_0 and r_1 aim at attenuating the impact of each LWR on the modelling of V_{gas}^0 (see Appendix 3). For Lanyon et al.'s LWR, the multiplier coefficient r_0 being close to 1 indicates that the rescaling procedure efficiently corrected most of the liner component of

the modelling error. The remaining correction consists merely of the addition of a constant volume of gas (r_1, m^3) to the model. This correction is moderate, when compared to the order of magnitude of the lungs volume ($\sim 4.5 \cdot 10^{-2} \text{m}^3$).

For the LWR obtained from cadavers, the values for the multiplier (r_0) indicate that the volume of gas remains slightly underestimated even the rescaling procedure. On the other hands, the offset r_1 is neglectable, due to the similar error trend for both allometry and LWR, that is underestimating both volumes and weight due to the use of cadavers in both cases.

4. Validation

In this chapter, the approximated values obtained from the parametric equations (Appendix 3) are used to solve simple case studies for the descending and ascending segment of a dive.

Unless stated otherwise, the figure corresponds to the case of a dugong with a body length equals to 2.6 m and a fineness ratio equals to 4.5. The air volume represents 105% of the modelled volume of the lungs (i.e. full lungs and air in the windpipe, see also paragraph Discrepancy between the selected and modelled neutral buoyancy depth z_n in the chapter METHODS) and the neutral buoyancy depth is selected to 0.75 m under the surface.

4.1. Change in buoyancy with depth

The buoyancy of a dugong immersed at a depth z is related to its density relative to the density of seawater. The adimensional relative density (ρ_{rel}) is:

$$\rho_{\text{rel}}(z) = 1 - \frac{\rho_w}{\rho_{\text{dugong}}^z} \tag{26}$$

The density of the dugong at depth z (ρ_{dugong}^z) is obtained by:

$$\rho_{\text{dugong}}^z = \frac{W_{BL}}{V_{\text{tot}}^z} \tag{27}$$

The expression of ρ_{rel} in terms of z and BL is obtained by inserting Eq. (27) into Eq. (26). The dependence of ρ_{rel} on BL is found to be neglectable (Fig. 4 left). In other words, the neutral buoyancy depth for dugongs of various BL is likely to be similar. Although never measured, no observation reported that the sub-surface depths where the dugongs swam, were correlated to their BL. The sensibility of ρ_{rel} to the neutral buoyancy depth (z_n) is shown on the right panel of Fig. 4.

As already stated, the behaviour of dugongs is beyond the scope of this paper. However, we assume that although they are able to dive deeper seafloor, dugongs forage preferentially shallow meadows due to the overall favourable energetic balance between energy consumed during the dives and gained by successful foraging. Assuming that dugongs spend most of their time near its neutral buoyancy depth, the reference (i.e. the most frequently experienced change in relative density) corresponds to the derivate of the relative density at neutral

Table 3

Error related to the selected length to weight relationship (LWR): Mean and standard deviation of the adimensional rescaling parameter (λ) for tested LWR, for male and female individuals and with transverse section of the trunk (TST) taller than wide (T-shaped) and wider than tall (W-shaped). The results presented here are calculated for body length ranging between 1.8 and 3.0 m and a selected neutral buoyancy depth $z_n = 1.0$ m. The fineness ratio ranges between 3.9 to 4.8, and the flattening (f) obtained as explained in the previous paragraph. The variables φ_{air} and φ_{methane} of the gas sub-model range between 1.05 and 1.20, and 0.0 and 0.2, respectively. φ_{luggs} is set to its average value (see Table 2).

	T-shaped		female		W-shaped		female	
	Male	Std (10^{-3})	Mean	Std (10^{-3})	male	Std (10^{-3})	Mean	Std (10^{-3})
Adulyanukosol et al.	1.005	0.131	1.006	0.128	1.005	0.133	1.006	0.129
Cherdsukjai et al.	1.004	0.771	1.006	0.073	1.004	0.774	1.006	0.074
Lanyon et al.	1.008	0.081	1.006	0.067	1.008	0.081	1.006	0.067
Nair et al.	1.006	0.207	1.006	0.528	1.006	0.221	1.006	0.536
Spain and Heinsohn	1.004	0.232	1.006	0.086	1.004	0.236	1.006	0.087

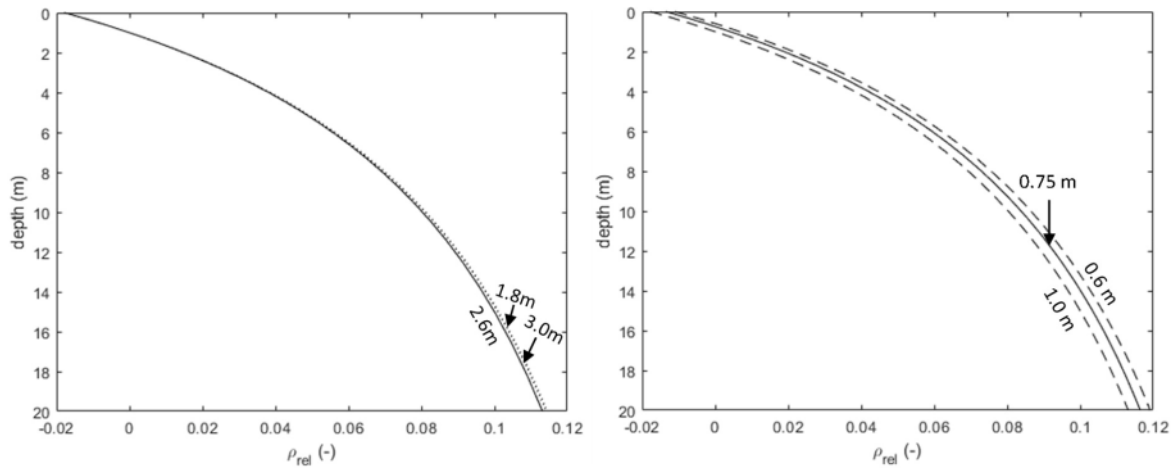


Fig. 4. Adimensional relative density of the dugong (ρ_{rel}) from the surface to depth of 20 m: (left) impact of the body length of a dugong (BL = 1.8, 2.6 and 3.0 m) on the relative density. (right) Sensibility of the relative density to the selected neutral buoyancy depth ($z_n = 0.6, 0.75$ and 1.0 m).

buoyancy depth ($\frac{\partial \rho_{rel}}{\partial z} |_{z=z_n}$). The divergence ($\frac{\partial \rho_{rel}}{\partial z} - \frac{\partial \rho_{rel}}{\partial z} |_{z=z_n}$) assesses how far the experienced change in buoyancy at a given depth z is from the one experienced around its neutral buoyancy depth. This divergence shown on Fig. 5 indicates that the depth where that divergence is small (i.e. where the relative density does not significantly vary from the one at the neutral buoyancy depth) corresponds to the depth range most frequently foraged.

4.2. Duration of descending phase

In this part, we examine the result of our model in the case of a dugong beginning a free sink (i.e. without swimming) with an initial null vertical velocity and a gravity centre lying slightly below its neutral buoyancy depth. The two depth-varying forces acting on the body are the drag force (F_D , Eq. (3)) and the buoyancy force (F_B , Eq. (4)). The adimensional drag coefficient C_D is comprised between 0.04 for streamlined bodies and 0.09 for half streamlined bodies.

With our hypothesis that the change in buoyancy is only due to the compression of gas-filled organs by the hydrostatic component of the water pressure, with Newton's second law of motion, the duration of a

free sink from just below the neutral buoyancy depth and a given depth is obtained by solving the differential equation:

$$W_{BL} \frac{\partial U(z)}{\partial t} = g(W_{BL} - \rho_w V_{tot}^0) + \rho_w g \frac{z}{z + z_{atm}} V_{gas}^0 - C_D \frac{\rho_w SA}{2} U(z)^2 \quad (28)$$

For a 2.6 m long adult dugong, the duration to attain the depth of 8.5 m from just below its neutral buoyancy depth will be comprised between 27 and 30 s. This estimation is consistent with the results in Chilvers et al. (2004) measured for same depth, in the case of the more regular dive type profiles; namely square, U-shaped and V-shaped. This estimation does not vary significantly for all tested values for φ_{air} and $\varphi_{methane}$ (Fig. 6).

The durations for free sinking dive from just below the neutral depth buoyancy and depths ranging from 2 to 20 m, for dugongs which BL range from 1.8 m to 3.0 m are presented on Fig. 7. The differences in durations is at most of few seconds between the smallest and largest individuals within the range of depths.

4.3. Energetic expenditure during the ascending phase

In this part, we examine the minimum amount of energy a dugong

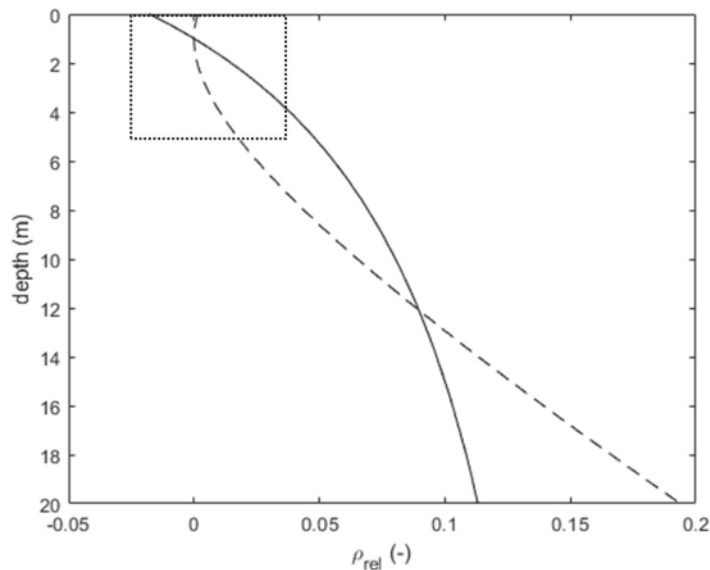


Fig. 5. Relative density (continuous line) and variation of the relative density with depth, relatively to the variation around the neutral buoyancy (divergence, dashed line). The dashed square highlights the depth range where the divergence does not vary significantly.

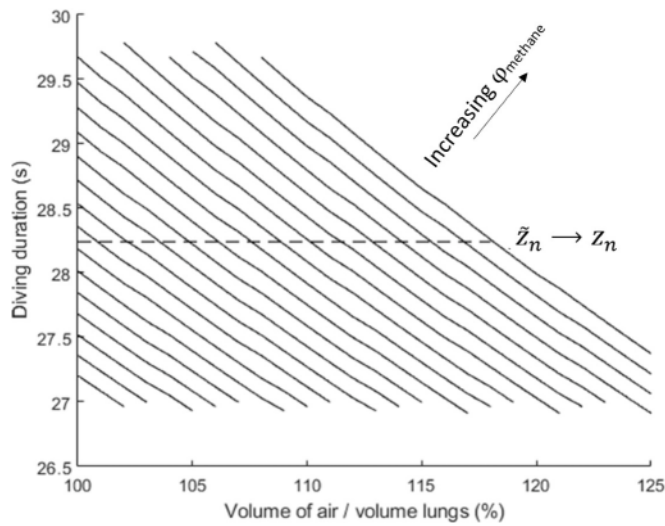


Fig. 6. Duration of a free sinking dive (no initial velocity) from immediately below the neutral depth with no initial velocity. The body length of the dugong is 2.6 m and the *a priori* selected neutral buoyancy depth $z_n = 1.0$ m. The ratio between the volume of air to the volume of lungs (φ_{air}) range from 1.00 to 1.25, and the ration between the volume of methane to the volume of intestines ($\varphi_{methane}$), from 0 to 0.20, (continuous lines). All results are obtained for data corresponding to a discrepancy between the *a priori* selected z_n and *a posteriori* value \tilde{z}_n (Eq. (23)) less than 10%. The horizontal dashed line corresponds to the same calculation using the optimal value for $\varphi_{methane}$ that ensure the convergence between a *a priori* and a *a posteriori* value for z_n (Eq. (25)).

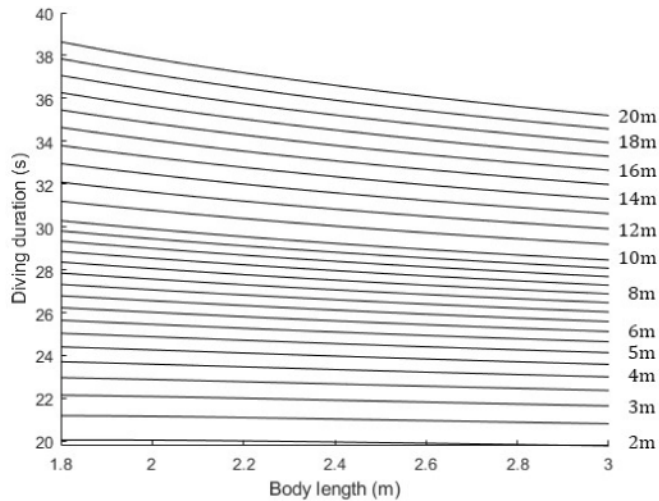


Fig. 7. Duration of free sinking dive (no initial velocity) from immediately below the neutral buoyancy depth to depths indicated on the right of the graph, and for dugongs with body length ranging from 1.8 m to 3.0 m.

must provide to travel back from the any depth up to the surface at a constant velocity. Since the buoyancy becomes positive for depths less than z_n , the segment between z_n and the surface does not consume any energy.

The effort that a dugong must provide to surface from the seafloor (z_{max}) is quantified by the work to be done from z_{max} to the neutral buoyancy depth z_n (Fig. 8). The work done by the depth varying buoyancy force between the depth z_{max} and z_n is:

$$Wk_B = \int_{z_{max}}^{z_n} F_B(z) dz \quad (29)$$

The work done by the depth-varying buoyancy force for a dugong of

given BL, ascending from a depth z to the neutral depth is obtained by integrating Eq. (29) with respect to z :

$$Wk_B = g(W_{BL} - \rho_w V_{tot}^0) \Delta z + \rho_{wg} V_{gas}^0 (\Delta z - z_{atm} (\log(z_n + z_{atm}) - (z_{max} + z_{atm}))) \quad (30)$$

with $\Delta z = z_n - z_{max}$.

Assuming a constant upward velocity U , the work done by the drag force is:

$$Wk_D = C_D \frac{\rho_w SA}{2} U^2 \Delta z \quad (31)$$

The minimum work needed to balance the work done by the drag and buoyancy forces along the trajectory between z_{max} and z_n is simply:

$$Wk_{ascent} = - (Wk_B + Wk_D) \quad (32)$$

Taking the constant upward velocity U equal to the free sinking velocity averaged between z_n and the corresponding depth, the power that a dugong must provide to ascend is:

$$\mathcal{P}_{ascent} = \frac{U Wk_{ascent}}{\Delta z} \quad (33)$$

In order to examine how energetically disadvantageous, the dive becomes with increasing depths, we compare the actual energetic expenditure for ascending and for swimming horizontally over the same distance, carried out at the neutral buoyancy depth (z_n) where no significant vertical component of the forces has to be compensated. The work done by the horizontal components of the thrust and drag force is:

$$Wk_{horiz} = (F_T + F_D) \Delta z \quad (34)$$

Dugongs swim by caudal oscillation described as carangiform with lunate tails (Webb, 1975; Marshall et al., 2022). The expression of the thrust force depends mostly of three parameters: the surface of its propulsive area, the amplitude of the stroke and their frequency (Lauder and Tytell, 2006; Kojeszewski and Fish, 2007; Fish et al., 2008). Although the mode of propulsion of manatee is described as sub-carangiform, we use the expression of the thrust force (F_T) developed for the manatees by Kojeszewski and Fish (2007) with all needed parameters approximated for dugongs with body length ranging from 1.8 m to 3.0 m. The horizontal velocity is taken equal to constant upward velocity U .

The ratio of Wk_{ascent} (Eq. (32)) on Wk_{horiz} (Eq. (34)) is shown on Fig. 9. It indicates how fast the amount of additional energy to consume for an ascending travel grows from the energy consumed to swim horizontally at the neutral buoyancy depth (i.e. with no buoyancy force to compensate) at the same velocity and over the same distance.

This increase in energetic expenditure is less dramatic for larger individuals than for the smaller ones. For example, in order to attain depth of 20 m, 3.0 m long dugong must consume ten times the amount of energy it spends when swimming horizontally whereas a 1.6 m long dugong will have to consume twenty times the energetic amount for its own horizontal swim.

5. Discussion

The tri-dimensional trajectory of a dugong during a diving cycle results of a series of actions such as swimming during brief sequences, gliding, orienting its fluke or body to modify its direction, slowing down by using their flippers. The choice of the succession of actions stems from the goal of a dugong: exploring an area, heading toward a specific location on the seafloor, shortening the diving duration, preventing to reach the seafloor too fast. As any motion, this trajectory can be expressed as the result of all the forces applied on a body. Some of these forces, depend on the dugong (swimming activity: thrust force, lift force) and some others do not (drag force). We hypothesized that the dugong has no control over the buoyancy force that solely varies due to the

compression of its gas-filled organs by the depth-changing water pressure.

It seems unlikely that the buoyancy remains constant: neither negative, which would force the dugongs to swim continuously to stay near the surface where they breathe, nor positive, which would prevent them to rest motionlessly or to crawl on the seafloor, as frequently observed. Moreover, for the buoyancy to remain constant, either the body must be incompressible, which is not ecologically sound, or a force must be produced to counterbalance the effect of the hydrostatic pressure, which would be energetically costly. For these reasons, we assume that the buoyancy not only changes with depth, but also is slightly positive at the surface and slightly negative on the seafloor, which implies that there must be a depth where it becomes neutral.

In few occurrences, large dugongs were reported sinking motionlessly tail-first from the surface after assuming an upright position (de Jongh et al., 1997; Anderson and Birtles, 1978). These observations are consistent with the notion of a buoyancy decreasing with depth. If initially, the gravity centre of dugong parallel to the surface is located near its neutral buoyancy depth, when assuming an upright position, the centre of gravity is moved below the neutral buoyancy depth. For the largest individuals, it can be sufficient to initiate a motion. For shorter individuals, the limited distance between the gravity centre and the neutral buoyancy depth generates a low initial velocity, which is probably the reason why they rely on the more efficient but more energetic demanding “roll” maneuver to initiate their dives.

The overall vertical component of the velocity can be approximated from duration measurements of travels between the surface and the seafloor at known depth, without possibility to distinguish the active to the free sinking component of velocity. We obtained modelled magnitudes of the free sinking velocity that represents a significant part of the overall vertical component of the velocity. It suggests that dugongs can rely primarily on the loss in buoyancy with depth to sink without any control over it. Dugongs are often observed using their flippers to slow down or incurving their trajectories in the vicinity of the seafloor as their velocity has become excessive. If dugongs could actually control their buoyancy, it is likely that they manage to maintain their velocities within acceptable limit.

This work aims at verifying that the novel hypothesis is consistent with the field observations and measurements from the literature. We formulate this hypothesis as a problem of physics, modelled it and solved it numerically. Three parameters related to the dugongs are involved: the surface envelope volume at the surface, the compressible to incompressible volume ratio at sea surface and the weight of the dugong. A new surface envelope model (SEM) based on allometry was developed. It improves significantly the model of Erdsack et al. (2018)

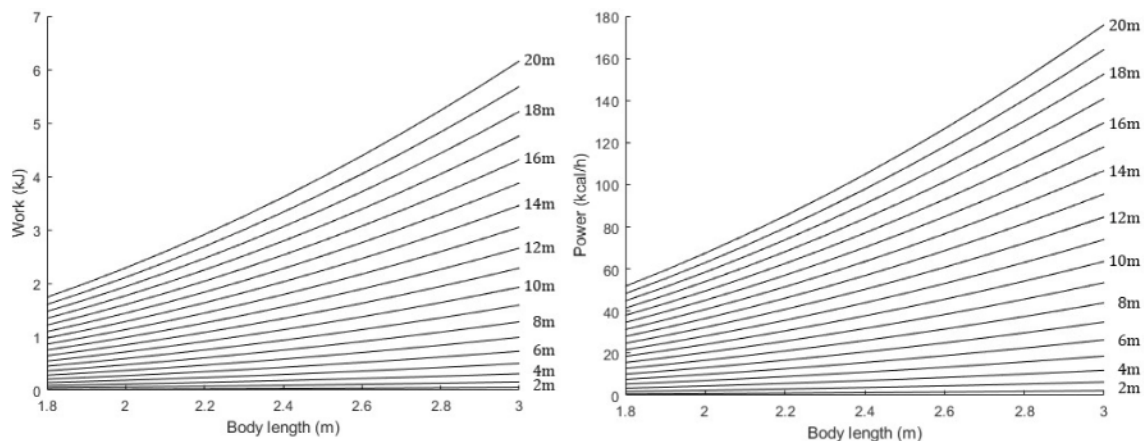


Fig. 8. (left) Work done by the buoyancy for dugongs with body length ranging from 1.8 m to 3.0 m ascending from the depth indicated on the right of the graph to z_n (right) minimum amount of energy consumed by dugongs with body length ranging from 1.8 m to 3.0 m when ascending at a constant velocity equal to the corresponding free sinking velocity (the power is converted in kcal/h).

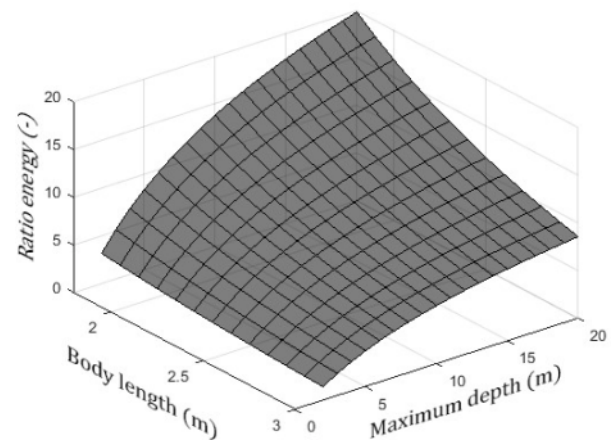


Fig. 9. Ratio of the work required to ascend from a given depth up to 20 m to the neutral buoyancy depth at constant velocity on the work done by swimming horizontally at the neutral buoyancy depth, over the same distance and at the same velocity, for dugongs with body length ranging from 1.8 m to 3.0 m.

for manatees as the sum of planar shapes and regular truncated cones. It offers an increased accuracy to evaluate the surface-area-to-volume-ratio which is a key parameter to assess the rate of thermal heat loss (Favilla et al., 2021). The weight is approximated by mean of a length to weight relationship (LWR) from the literature. The bias due to the use of allometry and of LWR obtained from cadavers was mitigated and led to an acceptable residual modelling error. Many data required to validate our hypothesis are either not available or subject to significant uncertainty. To circumvent this problem, different procedures were implemented. For example, Also, the values for each needed parameter was extended over a conservative “realistic range” based on educated guesses which can be seen as associating a very large uniform distribution for each used data. The model being solely the numerical translation of our hypothesis formulated from physics perspective, new data obtained with a more rigorous approach will contribute to refine our results by reducing the identified sources of errors.

The compressible volume being identified as the one occupied by gas, air and methane were considered in this study. The quantity of gas is supposed unchanged during the dive. If the compression of gas-filled organs by hydrostatic pressure compressed suffices to produce a free sinking at a velocity comparable to the overall measured vertical velocity, the reinflation of the gas volume during the ascending phase alleviates the cost of travel back to surface. It is sometimes suggested that dugongs could change their buoyancy by expelling gas. Our results

indicate that expelling gas is not only unnecessary to descend but also counterproductive to re-ascend. It is more likely that sirenians constantly expelling methane by relieving flatulence is not correlated to locomotion (Hartman, 1979).

The thick abdominal muscles of manatee were thought to be used to compress the methane trapped in the folds in the large intestine, and hence, contribute to buoyancy control (Rommel and Reynold, 2000). The compression of conservative” realistic” volume of methane impacts marginally the change in buoyancy with depth. However, this volume can significantly increase due to pathologic causes, resulting to an increase in positive buoyancy, and also in neutral buoyancy depth. In this case, it can happen that in this condition, the animal cannot achieve a “roll” maneuver energetically enough to attain the deeper buoyancy depth, and hence to initiate a free sink dive (Rommel and Reynold, 2000). Anyway, it is unlikely that dugongs rely on a gas that they can hardly ensure the required amount to be always available, for achieving vital activities such as reaching the seafloor to feed, or the surface to breath, contrarily to the air.

Dugongs initiate their dive after breathing in, lung full and with external nares closed by flap-like valves (Marsh et al., 1978). The benefit of keeping the air during the dive may appear counterintuitive since the major O₂ stores reside at the beginning of the dive within blood and tissues rather than lungs (Burggen, 1988). This apparent contradiction disappears with our hypothesis: the advantage of retaining air being to ensure the availability of a sufficient compressible volume.

Our hypothesis highlights the key role played by the neutral buoyancy depth. Dives are frequently initiated by a forcefully downward-directed motion (“roll”), consisting of the brief and energetic rotation near the surface. Such initial motion is required to counteract the positive buoyancy above the neutral buoyancy depth and to place the gravity centre enough below its neutral buoyancy depth to initiate a free sink dive. Moreover, the “roll” maneuver also provides a momentum that adds up to the one due to the action of the gravity. Ascending dives beginning with a brief push against the seafloor were reported (Shawky and Daoud, 2017). Our estimations of the work to be done for ascending from various depth to the surface indicates that the energetic amount required to ascend is limited. The momentum produced by this initial push may suffice to reach the surface from shallow depth or must be completed by subsequent brief fluke strokes and glide sequences for

deeper travels.

6. Conclusion

We propose the novel hypothesis on how dugongs manage to travel along the water column with very little activity. We assumed that dugongs take advantage of the change in buoyancy due to the compression of their gas-filled organs by the depth-changing water pressure. This hypothesis was modelled in terms of physics and the model was run for various sets of parameters describing specific features of this species. Solutions were found for dugongs slightly positively buoyant at sea surface and becoming neutrally buoyant at a very shallow depth below the surface where they are observed floating motionlessly. The gradual loss in buoyancy under the neutral buoyancy depth was assessed and served to calculate the vertical component of the velocity for free sink dive from bellow the neutral buoyancy depth to the depths foraged by the dugongs was calculated. The corresponding modelled durations were close to the few measured ones. Finally, we showed that the energetic expenditure required to travel back from the seafloor to the surface was moderate for the preferred range for foraging but increased sharply with increasing depth. The modelling of the change in buoyancy only due to the compression of their gas-filled organs by the depth-changing water pressure allows to replicate observed behaviours such as motionless floating below the surface, sinking tail-first for larger individuals, resting against the seafloor sinking and travelling with a very few or even no swimming activity, either downward after an initial “roll” or upward, after an initial push against the seafloor. This novel hypothesis should be taken into consideration in future research.

CRedit authorship contribution statement

Jean-Pierre Lefebvre: Conceptualization, Methodology, Software, Validation, Writing – original draft.

Declaration of Competing Interest

The author declares that he has no known competing financial interests or personal relationships that could have appeared to influence the work reported in this paper.

Appendix 1: Calculation of volume and surface area of for the flat appendages

Flippers

The surface area of the two flippers is estimated from the flipper length and width allometry, assuming a half elliptic contour shape:

$$SA_{flippers} = 2\pi L_{flipper} W_{flipper} \tag{A1.1}$$

The corresponding volume, assuming a constant thickness T_{ff} is:

$$V_{flippers} = \frac{1}{2} T_{ff} SA_{flippers} \tag{A1.2}$$

Fluke

The area of the propulsive surface is central for the calculation of swimming kinetics of the dugong. For this reason, the shape of the fluke is modelled as accurately as possible, from four parameters issued from the allometry equations: L_{fluke} , W_{fluke} , L_{notch} and $G_{basetail}$.

The surface area of the fluke is evaluated by means of three points: A, B and C in the coordinate system $[O, \vec{x}, \vec{y}]$ (Fig. A1.1). The coordinates of the point A at the junction of anterior and posterior edge of the fluke are:

$$A_{xOy} = \begin{bmatrix} 0.5 W_{fluke} \\ -L_{notch} \end{bmatrix} \tag{A1.3}$$

with W_{fluke} the maximum posterior width of the tail fluke and L_{notch} , the distance from the apex of the notch to a line joining the posterolateral tips of the fluke.

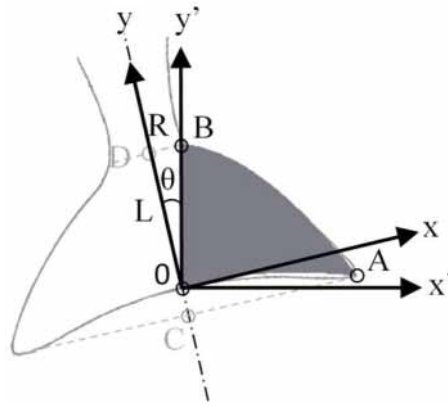


Fig. A1.1. Approximation of the shape of the section of the fluke extending outside the tail.

All points are then expressed in the coordinate system $[O, \vec{x}', \vec{y}']$, obtained by rotation clockwise of an angle θ around O of $[O, \vec{x}, \vec{y}]$, so that, the abscise of B is null in this rotated system:

$$B_{x'Oy'} = \begin{bmatrix} 0 \\ L_{fluke} \end{bmatrix} \tag{A1.4}$$

With L_{fluke} , the distance from the base of the tail fluke to the apex of its median notch. The distance $\|\overline{BD}\|$ being equal to the radius (R) of the base of the tail girth, from Eq. (2):

$$\theta = -asin \frac{K(\alpha, \beta) G_{base\ tail}}{L_{fluke}} \tag{A1.5}$$

The coordinates of A in the rotated coordinate system are:

$$A_{x'Oy'} = \begin{bmatrix} \frac{W_{fluke}}{2} \cos\theta + N_{fluke} \sin\theta \\ \frac{W_{fluke}}{2} \sin\theta - N_{fluke} \cos\theta \end{bmatrix} \tag{A1.6}$$

The equation for the contour of both the anterior and the posterior edge of the fluke is expressed as:

$$y' = a x'^m + b \tag{A1.7}$$

The coefficients are chosen to simulate the curves of the anterior and posterior contour ($n = 1.75$ and 1.95 , respectively). For $x' = 0$, the curves of the anterior and posterior contour passing by the point C and B, respectively, $b_{ant} = 0$ and $b_{pos} = L$. The coefficients a_{ant} and a_{pos} are obtained at the point A.

The surface area of the fluke (i.e. cumulated left and right parts) is obtained as:

$$SA_{fluke} = 4 \int_0^{x_A} y_{pos} - y_{ant} dx_{\theta} \tag{A1.8}$$

The associated volume of the fluke is obtained with a constant thickness:

$$V_{fluke} = 0.5 T_{ff} SA_{fluke} \tag{A1.9}$$

The one-sided propulsive area of the fluke is:

$$PA_{fluke} = \frac{SA_{fluke}}{2} + L.R \tag{A1.10}$$

If the second term L.R is neglected, the propulsive area of the fluke is entirely defined by allometry.

Appendix 2: Calculation of volume and surface area of for segments generated by a revolution about the longitudinal axis

The equations for assessing the volumes and surface areas, when they exist, are provided for the snout, the head and the trunk.

Snout

Assuming that the contour of the transverse section at the base of the snout is approximately circular, its shape is modelled as a semi-oblate ellipsoid of radius R_{snout} and height x_0 . The corresponding volume and surface area are calculated with the canonical equations:

$$V_{snout} = \frac{2\pi}{3} x_0 R_{snout}^2 \tag{A2.1}$$

$$SA_{snout} = \pi R_{snout} \left(R_{snout} + x_0 \frac{\arccos \frac{R_{snout}}{x_0}}{\sqrt{1 - \arccos^2 \frac{R_{snout}}{x_0}}} \right) \tag{A2.2}$$

Head

The shape of the head is modelled as an irregular truncated cone with a circular section in the transverse plan at the snout to elliptic section in the transverse plan at the neck. At the base of the snout (x_{snout}), the shape factors are $\alpha(x_{snout}) = 1$, $\beta(x_{snout}) = 1$ and the scaling radius (R_{snout}) is obtained from the size allometry for G_{snout} :

$$R_{snout} = \frac{1}{2\pi} G_{snout} \tag{A2.3}$$

At the anterior neck (x_{neck}), $\alpha(x_{neck}) = \alpha$, $\beta(x_{neck}) = \beta$ and the scaling radius at the neck (R_{neck}) is obtained from the size allometry for G_{neck} :

$$R_{neck} = K(\alpha, \beta) G_{neck} \tag{A2.4}$$

Assuming that the shape factors s (α and β) vary linearly over a distance from the snout to the neck noted L_{head} :

$$s(x) = (s - 1) \frac{x}{L_{head}} + 1 \tag{A2.5}$$

The corresponding semi-axis lengths L_s (L_α in the sagittal and L_β in the frontal plane) are:

$$L_s(x) = (s(x) R_{neck} - R_{snout}) \frac{x}{L_{head}} + R_{snout} \tag{A2.6}$$

Combining these two equations, the semi-axis is rewritten as a second order polynomial of x :

$$L_s(x) = a(s - 1)x^2 + bx + b \tag{A2.7}$$

With $a = \frac{R_{neck}}{L_{head}^2}$, $b = \frac{R_{neck} - R_{snout}}{L_{head}}$ and $c = R_{snout}$
 The area of the transverse section at any distance x from the base of the snout is obtained with the sum of the two half-ellipses $\mathcal{E}(\alpha, \beta)$ and $\mathcal{E}(\alpha, 1)$ expressed as a 4th order polynomial of x :

$$A_{\alpha,\beta}(x) = \frac{\pi}{2} L_\alpha(x) L_\beta(x) + \frac{\pi}{2} L_\alpha(x) L_1(x) \tag{A2.8}$$

The corresponding volume is obtained by integrating $A_{\alpha,\beta}(x)$ along x over L_{head} :

$$V_{head}^{\alpha,\beta} = \int_0^{L_{head}} A_{\alpha,\beta}(x) dx \tag{A2.9}$$

Trunk

The surface area of the transversal section at length l within the trunk is:

$$\int_0^{2\pi} S(\ell, \theta) d\theta = A_{\alpha,\beta}(\ell) = \frac{\pi}{2} \alpha(\beta + 1) R(\ell)^2 \tag{A2.10}$$

The corresponding volume is:

$$V = C(\alpha, \beta) \int_{AptCommandmathcall_1}^{AptCommandmathcall_2} G^2(\ell) d\ell \tag{A2.11}$$

with $C(\alpha, \beta) = \frac{2}{\pi} \alpha(1 + \beta)(K_{\alpha,1} + K_{\alpha,\beta})^{-2}(\alpha, \beta)$

Appendix 3: Parametric equations

In this part, we present the coefficients of the parametric equations for the five parameters in Eqs. (2)-(9): total (V_{tot}^0, m^3) and gas volume (V_{gas}^0, m^3), at still water level (SWL), the propulsive area of the fluke (PA_{fluke}, m^2) and of the two flippers ($PA_{flippers}, m^2$) and the total surface area (SA, m^2) of a dugong of a given body length (BL). The expressions of two additional parameters involved in the approximation for the gas volume at SWL are also provided: the intestines ($V_{intestines}^0, m^3$) and lungs volume (V_{lungs}^0, m^3).

All the coefficients are determined by fitting in a least square sense, a type of function of a selected type (i.e. the parametric equation of a given parameter, Table A3.1) to a selection of variables (i.e. the ‘‘explanatory variables’’) from the N sets of independent parameters with all solutions obtained for both sexes merged together (Tables A3.2-A3.6).

Table A3.1

Expression of the parametric equations for the seven parameters required to quantify the motion of a dugong along the water column with its governed buoyancy by the depth-varying hydrostatic pressure. (left column) definition and units of the parameters, (center) abbreviation of the parameter as used in the text. The superscript ⁰ indicates that the parameter is approximated at the still water level. When omitted, it indicates that the parameter can be taken as independent of depth (right column) expression of the parametric equation. All coefficients are dimensionless, except r_1 (kg).

Propulsive area of the fluke	(m ²)	PA _{fluke}	$b BL^c$
Propulsive area of the two flippers	(m ²)	PA _{flippers}	$d BL^e$
Volume of intestines	(m ³)	V _{intestines} ⁰	$f BL^h$
Total volume	(m ³)	V _{tot} ⁰	$k_{00} + k_{10} BL + k_{01} FR + k_{11} BL FR + k_{20} BL^2$ with $k_{ij} = l_{ij}z_n + m_{ij}$
Total surface area	(m ²)	SA	$n(V_{tot}^0 - T_{ff} PA_{ff})^o + 2 PA_{ff}$ with $PA_{ff} = PA_{fluke} + PA_{flippers}$
Volume of the lungs	(m ³)	V _{lungs} ⁰	$p \hat{V}_{tot}^o q$
Gas volume	(m ³)	V _{gas} ⁰	$r_0 (\varphi_{air} V_{lungs}^0 + \varphi_{methane} V_{intestines}^0) + r_1$

The coefficients of determination (r^2) indicated in the tables below are calculated with the modelled and parametrized value of each parameter. They assess how well, the parametrized equations reflect the modelled data, and by no means, how close the modelled or parametrized data are from measurements. All these coefficients are dimensionless, but the offset parameter r_1 (m³). When the parametrized equation is identical to the modelled one, that is, when the parameter is fully described by allometric equation, the mention $r^2 = 1$ is omitted.

Parametric equations dependent of BL only

Three parameters can be considered as independent of the shape factors: the propulsive area of the fluke (see remark in Appendix 2 for PA_{fluke}), the propulsive area of the two flippers and the volume of the small and large intestine . The corresponding equations are obtained from allometry (Table A3.2).

Table A3.2

Coefficients of the parametric equation for the propulsive area of the fluke (PA_{fluke}, Eq. (19)), of the two flippers (PA_{flippers}, Eq. (20)) and of the volume of the small and large intestine (V_{intestines}, Eq. (21)).

Propulsive area of the fluke (m ²)	
b (10 ⁻²)	3.3095
C	1.9641
r ²	0.9974
Propulsive area of the two flippers (m ²)	
d (10 ⁻²)	1.9853
E	1.8230
Volume of the small and large intestine (m ³)	
f (10 ⁻²)	1.7509
h	1.4358

Parametric equations of depth-dependent volumes and surface areas

The coefficients of the parametric equations for the total volume at sea surface, the total surface area, the lung volume and gas volume at sea surface are reported in tables A3.3, A3.4, A3.5 and A3.6, respectively. These coefficients are assessed for every length to weight relationships (LWR) but for Nair et al. (1975).

Table A3.3

Coefficients for the parametric equation (Eq. (22)) for the total volume at sea surface (V_{tot}⁰). For each coefficient, the value in the upper part of the box corresponds to the T-shaped case, and tin the lower part, to the W-shaped case. Each coefficients k_{ij} are linearly related the neutral buoyancy depth (z_n) through the pair of associated coefficients in the second column (l_{ij} and m_{ij}, Eq. (23)).

		Total volume at surface sea (m ³)			
		Adulyanukosol et al	Cherdukjai et al.	Lanyon et al.	Spain and Heinsohn
k00 (10 ⁻³)	l00	3.1146	1.4328	1.9392	0.2166
	m00	2.9580	1.2386	1.6626	0.0293
k10 (10 ⁻³)	l10	154.1564	43.1754	56.3876	-33.4667
		154.2883	43.1993	56.4174	-33.4733
	m10	-3.7160	-1.5440	-2.0501	-0.7387
		-3.6542	-1.4620	-1.9377	-0.6673
k01 (10 ⁻³)	l01	-204.8299	-65.1662	-85.7333	-14.6652
		-204.8149	-65.1584	-85.7228	-14.6615
	m01	-0.0254	-0.0289	-0.0418	-0.0291
		0.0049	0.0089	0.0130	0.0093

(continued on next page)

Table A3.3 (continued)

		Total volume at surface sea (m ³)			
		Adulyanukosol et al	Cherdukjai et al.	Lanyon et al.	Spain and Heinsohn
k11 (10 ⁻³)	m01	-0.0901	-0.0218	-0.0284	-0.0011
		-0.1821	-0.0421	-0.0545	0.0003
	l11	0.0065	0.0081	0.0117	0.0079
k20 (10 ⁻³)		-0.0026	-0.0042	-0.0060	-0.0044
	m11	0.0196	0.0049	0.0064	0.0003
		0.0710	0.0164	0.0212	-0.0002
	l20	1.6227	1.0236	1.4028	0.9494
		1.6174	1.0127	1.3906	0.9445
	m20	96.5981	58.5425	81.5688	54.0032
		96.5472	58.5290	81.5512	54.0013
r ²		1.0000	1.0000	1.0000	1.0000

Table A3.4

Coefficients for the parametric equation (Eq. (24)) for the total surface area (SA). The thickness of the flat appendages (T_{ff}) is taken equal to 0.05 m.

		Total surface area (m ²)			
		Adulyanukosol et al	Cherdukjai et al.	Lanyon et al.	Spain and Heinsohn
N		5.66155	5.37496	5.8249	5.5580
o		0.63858	0.60304	0.6159	0.6157
r ²		0.9824	0.9749	0.9745	0.9774

Table A3.5

Coefficients for the parametric equation (Eq. (25)) for the total volume of the lungs at sea surface (V_{lungs}).

		Volume of lungs at sea surface (m ³)			
		Adulyanukosol et al	Cherdukjai et al.	Lanyon et al.	Spain and Heinsohn
p (10 ⁻¹)		2.2617	2.2189	1.488529	2.0511
q		1.06498	1.06485	1.06462	1.05414

Table A3.6

Coefficients for the parametric equation (Eq. (26)) of the total volume of gas at sea surface (m³).

		Volume of gas (air + methane) at sea surface (m ³)			
		Adulyanukosol et al	Cherdukjai et al.	Lanyon et al.	Spain and Heinsohn
r ₀		0.7128	0.71392	1.0201	0.7686
r ₁ (10 ⁻³) (m ³)		0.7575	1.3970	2.0448	0.8928
r ²		0.9998	0.9991	0.9990	0.9995

Chapter methods

Dimensional parameters

BL	m	Body length
g	m.s ⁻²	Acceleration due to gravity
G	m	Girth
l	m	Length along the longitudinal axis, from the tip of the snout to apex of the notch in the tail fluke
P	Pa	Pressure
PA	P _{air}	Pressure in the airways
	P _h	Hydrostatic pressure
	m ²	Propulsive area
	PA _{flippers}	Propulsive area of the two flippers
R	PA _{fluke}	Propulsive area of the fluke
	PA _{ff}	Propulsive area of the fluke and the two flippers
	m	Scaling radius
SA	m ²	Total surface envelope area
T _{ff}	m	Thickness of the flat appendages (fluke and flippers)
T _{max}	m	Maximum thickness in the transverse planes
V	m ³	volume
	V _{air}	Volume of air
	V _{intestines}	Volumes of the small and large intestine
	V _{lungs}	Volume of the lungs
	V _{methane}	Volume of methane

(continued on next page)

(continued)

	V_{nta}	Volume of the neck-thorax/abdomen segment
	V_{sa}	Volume of air in incompressible storages
	V_{tot}	Total volume of the surface envelope
W	kg	weight
	W_{BL}	Weight estimated by a length-weight relationship for a given BL
z	m	depth measured from the still water level (SWL)
	z_{max}	Depth of the seafloor
	z_n	Neutral buoyancy depth

Adimensional parameters

f	Flattening of the trunk
FR	Fineness ratio of the trunk
α	Ratio between the ellipse radius in the frontal plane to the scaling radius (R)
β	Ratio between the ellipse radius in the sagittal plane to the scaling radius (R)
λ	Adimensional rescaling parameter
φ	Volume ratio at sea surface
φ_{air}	Ratio between the volume of the air and the volume of the lungs at sea surface
φ_{lungs}	Ratio between the volume of the lungs and the volume of the neck-thorax/ abdomen at sea surface
$\varphi_{methane}$	Ratio between the volume of the methane and the volume of the intestine at sea surface

Fitting coefficients (Appendix 3)

a_0 to a_5	–	Coefficients of the foil equation
b, c	–	Parametric equation for the propulsive area of the fluke
d, e	–	Parametric equation for the propulsive area of the flippers
f, h	–	Parametric equation for the volume of the intestines
k_{ij}	–	Parametric equation for the total volume at sea surface
l_{ij}, m_{ij}	–	Dependence of k_{ij} on z_n
n, o	–	Parametric equation for the total surface area
p, q	–	Parametric equation for the volume of the lungs at sea surface
r_0	–	Multiplier of the parametric equation for gas volume at sea surface
r_1	m^3	Offset of the parametric equation for gas volume at sea surface

Chapter validation

Dimensional parameters

F_B	N	Buoyancy force
F_D	N	Drag force
F_T	N	Thrust force
φ_{ascent}	$kcal.h^{-1}$	Power needed to ascent
U	$m.s^{-1}$	Vertical component of the velocity
Wk	kJ	work
	Wk_B	Work done by the buoyancy force
	Wk_D	Work done by the drag force
ρ_{dugong}	$kg.m^{-3}$	Density of a dugong at depth z

Adimensional parameters

C_D	–	Drag coefficient
ρ_{rel}	–	Density of a dugong relatively to the seawater

Constants

g	9.81	$m.s^{-2}$	Acceleration due to gravity
P_{atm}	101,325	Pa	Atmospheric pressure at sea level
ρ_w	1021	$kg.m^{-3}$	Seawater density

Conventions

Superscripts	
0	Parameter estimated at sea surface
z_n	Parameter estimated at neutral buoyancy depth
Z	Parameter estimated at depth z
average	Average value for an independent variable
opti	Optimal value for the minimization of a modelling error
\tilde{z}_n	A posteriori estimator for the neutral buoyancy depth (z_n)

Other abbreviations

LWR	Length to weight relationship
PCC	Pearson Correlation Coefficient
SEM	Surface envelope model
TTS	Transverse trunk section

References

- Adulyanukosol, K., Prasittipornkul, C., Man-Anansap, S., Boukaew, P., 2009. Stranding records of dugong (*Dugong dugon*) in Thailand. In: Proc. 4th Int. Symp. on SEASTAR2000 and Asian Bio-logging Science (8th SEASTAR2000 workshop), pp. 51–57.
- Amamoto, N., Ichikawa, K., Arai, N., Akamatsu, T., Shinke, T., Adulyanukosol, K., 2009. The depth of water effects the feeding ground selection by dugongs in dry season. *J. Adv. Mar. Sci. Technol. Soc.* 15 (2), 149–157.
- Anderson, P.K., 1981. The behaviour of the Dugong (*Dugong dugon*) in relation to conservation and management. *Bull. Mar. Sci.* 3 (31), 640–647.
- Anderson, P.K., Birtles, A., 1978. Behaviour and ecology of the dugong *Dugong dugon* (Sirenia): observations in Shoalwater and Cleveland Bays, Queensland. *Aust. Wildlife Res.* 5, 1–23.
- Aoki, K., Watanabe, Y.Y., Crocker, D.E., Robinson, P.W., Biuw, M., Costa, D.P., Miyazaki, N., Fedak, M.A., Miller, P.J.O., 2011. Northern elephant seals adjust gliding and stroking patterns with changes in buoyancy: validation of at-sea metrics of body density. *J. Exp. Biol.* 214, 2973–2987. <https://doi.org/10.1242/jeb.055137>.
- Bayliss P., Raudino H., Hutton M., Murray K., Waples K., Strydom S. (2019) Modeling the spatial relationship between dugong (*Dugong dugon*) and their seagrass habitat in Shark Bay Marine Park before and after the marine heatwave of 2010/11. Dugongs & seagrass NESP, final report, 55 pp.
- Brakes, P., Dall, S.R.X., 2016. Marine mammal behavior: a review of conservation implications. *Front. Mar. Sci.* 3, 87. <https://doi.org/10.3389/fmars.2016.00087>.
- Brown, R.E., Butler, J.P., 2000. The absolute necessity of chest-wall collapse during diving in breath-hold diving mammals. *Aquat. Mamm.* 26 (1), 26–32.
- Burggen, W., 1988. Cardiovascular responses to diving and their relation to lung and blood oxygen stores in vertebrates. *Can. J. Zool.* 66, 20–28.
- Cherdokjai, P., Buddhachat, K., Brown, J., Kaewkool, M., Poomouang, A., Kaewmong, P., Kittiwattawanong, K., Nganvongpanit, K., 2020. Age relationships with telomere length, body weight and body length in wild dugong (*Dugong dugon*). *PeerJ* 8, e10319. <https://doi.org/10.7717/peerj.10319>.
- Chilvers, B.L., Delean, S., Gales, N.J., Holley, D.K., Lawler, I.R., Marsh, H., Preen, A.R., 2004. Diving behaviour of dugongs, *Dugong dugon*. *J. Exp. Mar. Biol. Ecol.* 304, 203–224. <https://doi.org/10.1016/j.jembe.2003.12.010>.
- Cotten, P.B., Piscitelli, M.A., McLellan, W.A., Rommel, S.A., Dearolf, J.L., Pabst, D.A., 2008. The gross morphology and histochemistry of respiratory muscles in bottlenose dolphins, *Tursiops truncatus*. *J Morphol* 269 (12), 1520–38. <https://doi.org/10.1002/jmor.10668>.
- de Iongh, H.H., Bierhuizen, B., van Orden, B., 1997. Observations on the behaviour of the dugong (*Dugong dugon* Müller, 1776) from waters of the Lease Islands, eastern Indonesia. *Contrib. Zool.* 67 (1), 71–77.
- Domning, D.P., De Buffrénil, V., 1991. Hydrostatics in the Sirenia: quantitative data and functional interpretations. *Mar. Mamm. Sci.* 7 (4), 331–368.
- D'Souza, E., Patankar, V., 2009. First underwater sighting and preliminary behavioural observations of Dugongs (*Dugong dugon*) in the wild from Indian waters, Adaman Islands. *J. Threat. Taxa* 1 (1), 49–53.
- Erdsack, N., McCully Phillips, S.R., Rommel, S.A., Pabst, D.A., McLellan, W.A., Reynolds III, J.E., 2018. Heat flux in manatees: an individual matter and a novel approach to assess and monitor the thermal state of Florida manatees (*Trichechus manatus latirostris*). *J. Comp. Physiol. B.* <https://doi.org/10.1007/s00360-018-1152-7>.
- Fahlman, A., Loring, S.H., Ferrigno, M., Moore, C., Early, G., Niemeyer, M., Lentell, B., Wenzel, F., Joy, R., Moore, M.J., 2011. Static inflation and deflation pressure-volume curves from excised lungs of marine mammals. *J. Exp. Biol.* 214, 3822–3828. <https://doi.org/10.1242/jeb.056366>.
- Favilla, A.B., Horning, M., Costa, D.B., 2021. Advances in thermal physiology of diving mammals: the dual role of peripheral perfusion. *Temperature* 21. <https://doi.org/10.1080/23328940.2021.1988817>.
- Fish, F.E., 1993. Influence of hydrodynamic design and propulsive mode on mammalian swimming energetics. *Aust. J. Zool.* 42, 79–101.
- Fish, F.E., Howle, L.E., Murray, M.M., 2008. Hydrodynamic flow control in marine mammals. *Integr. Comp. Biol.* 48 (6), 788–800. <https://doi.org/10.1093/icb/ict029>.
- Hartman, D.S., 1979. Ecology and behaviour of the manatee (*Trichechus manatus*) in Florida. The American Society of Mammologists, Special Publication, 5, p. 151.
- Hodgson, A.J., 2004. Dugong Behaviour and Responses to Human Influences, PhD thesis, School of Tropical Environment Studies and Geography. James Cook University, Townsville, Australia, p. 271.
- Jung, S., 2021. Swimming, flying, and diving behaviors from a unified 2D potential model. *Nat. Portfolio Sci. Rep.* 11, 15984. <https://doi.org/10.1038/s41598-021-94829-7>.
- Kojeszewski, T., Fish, F.E., 2007. Swimming kinematics of the Florida manatee (*Trichechus manatus latirostris*): hydrodynamic analysis of an undulatory mammalian swimmer. *J. Exp. Biol.* 210, 2411–2418. <https://doi.org/10.1242/jeb.02790>.
- Lanyon, J.M., 1991. The Nutritional Ecology of the Dugong (*Dugong dugon*) in Tropical North Queensland. Ph.D. Thesis. Department of Ecology and Evolutionary Biology, Monash University, Melbourne, Australia, p. 337.
- Lanyon, J.M., Sneath, H.L., Long, T., Bonde, R.K., 2010. Physiological response of wild dugongs (*Dugong dugon*) to out-of-water sampling for health assessment. *Aquatic mammals* 36 (1), 46–58. <https://doi.org/10.1578/AM.36.1.2010.46>.
- Lauder, G.V., Tytell, E.D., 2006. Hydrodynamics of undulatory propulsion. *Fish Biomech.* (23) *Fish Physiol.* 11, 425–468. [https://doi.org/10.1016/S11546-5098\(05\)23011-X](https://doi.org/10.1016/S11546-5098(05)23011-X).
- Marsh H. (1989) Dugongidae in fauna of Australia eds. Walton and Richardson, 57, 18 pp.
- Marsh, H., Saalfeld, W.K., 1989. Distribution and abundance of dugongs in the northern Great Barrier Reef marine park. *Aust. Wildlife Res.* 16, 429–440.
- Marsh, H., Sobotzick, S., 2019. *Dugong dugon* (amended version of 2015 assessment). In: The IUCN Red List of Threatened Species 2019: e.T6909A160756767. <https://doi.org/10.2305/IUCN.UK.2015-4.RLTS.T6909A160756767.en>.
- Marsh, H., Spain, A.V., Heinsohn, G.E., 1978. Physiology of the dugong. *Comp. Biochem. Physiol.* 16A, 159–168.
- Marshall, C.D., Sarko, D.K., Reep, R.L., 2022. Morphological and sensory innovations for an aquatic lifestyle. In: Würsig, B. (Ed.), *Ethology and Behavioural Ecology of Sirenia. Ethology and Behavioural Ecology of Marine Mammals*. Series. Springer, pp. 23–27. https://doi.org/10.1007/978-3-030-90742-6_ededMarsh_§2.
- Mayor, S.J., Schneider, D.C., Schaefer, J.A., Mahoney, S.P., 2009. Habitat selection at multiple scales. *Ecoscience* 16 (2), 238–247. <https://doi.org/10.2980/16-2-3238>.
- Miller, P.J.O., Johnson, M.P., Tyack, P.L., Terray, E.A., 2004. Swimming gaits, passive drag and buoyancy of diving sperm whales *Physeter microcephalus*. *J. Exp. Biol.* 207, 1953–1967. <https://doi.org/10.1242/jeb.00993>.
- Mishra, A.K., Narayana, S., Apte, D., 2021. Loss of Dugong grass [*Halophila ovalis* (R. Brown)] population structure due to habitat disturbance in an island ecosystem. *Indian J. Geo Mar. Sci.* 50 (2), 115–121.
- Moore, C., Moore, M., Trumble, S., Niemeyer, M., Lentell, B., McLellan, W., Costidis, A., Fahlman, A., 2014. A comparative analysis of marine mammal tracheas. *J. Exp. Biol.* 217, 1154–1166. <https://doi.org/10.1242/jeb.093146>.
- Nair, R.V., Lal Mohan, R.S., Satyanarayana Rao, K., 1975. The dugong *Dugong dugon*. *ICAR. Bull. Central Mar. Fish. Res. Inst.* 26, 45.
- Nowacek, D.P., Johnson, M.P., Tyack, P.L., Shorter, K.A., McLellan, W.A., Pabst, D.A., 2001. Buoyant Balaenids: the ups and downs of buoyancy in right whales. *Proc.: Biol. Sci.* 268 (1478), 1811–1816. <https://doi.org/10.1098/rspb.2001.1730>.
- Pabst, D.A., Rommel, S.A., McLellan, W.A., 1999. The functional morphology of marine mammals. *Biology of Marine Mammals*. Smithsonian Institution press, p. 1454. Reynold III and Rommel (eds.).
- Rommel, S., Reynolds III, J.E., 2000. Diaphragm structure and function in the Florida manatee (*Trichechus manatus latirostris*). *Anat. Rec.* 259, 41–51.
- Shawky A.M., Daoud, M.E.-S. (2017) Effect of tourism activities on the behavioural ecology of *Dugong dugon* inhabiting Marsa Alam, Red Sea, Egypt. Update November 2017, 3 pp.
- Sheppard, J.K., Preen, A.R., Marsh, H., Lawler, I.R., Whiting, S.D., Jones, R.E., 2006. Movement heterogeneity of dugongs, *Dugong dugon* (Müller), over large spatial scales. *J. Exp. Mar. Biol. Ecol.* 334, 64–83. <https://doi.org/10.1016/j.jembe.2006.01.011>.
- Skrovan, R.C., Williams, T.M., Berry, P.S., Moore, P.W., Davis, R.W., 1999. The diving physiology of bottlenose dolphins (*Tursiops truncatus*). II. Biomechanics and changes in buoyancy at depth. *J. Exp. Biol.* 202, 2749–2761.
- Spain, A.V., Heinsohn, G.E., 1975. Size and weight allometry in a North Queensland population of *Dugong dugon* (Müller) (Mammalia: sirenia) Australian. *J. Zool.* 23, 159–168.
- Tenney, S.M., Remmers, J.E., 1963. Comparative quantitative morphology of the mammalian lung: diffusing area. *Nature* 197 (4862), 54–56.
- Thums, M., Bradshaw, C.J.A., Sumner, M.D., Horsburgh, J.M., Hindell, M.A., 2013. Depletion of deep marine food patches forces divers to give up early. *J. Anim. Ecol.* 82, 72–83. <https://doi.org/10.1111/j.1365-2656.2012.02021.x>.
- Tol, S.J., Coles, R.G., Congdon, B.C., 2016. *Dugong dugon* feeding in tropical Australian seagrass meadows: implications for conservation planning. *PeerJ* 4, e2194. <https://doi.org/10.7717/peerj.2194>.
- Trassinelli, M., 2016. Energy cost and optimisation in breath-hold diving. *J. Theor. Biol.* 396, 42–45. <https://doi.org/10.1016/j.jtbi.2016.02.009>.
- Villarino, M.B., 2006. A note on the accuracy of Ramanujan's approximative formula for the perimeter of an ellipse. *J. Inequal. Pure Appl. Math.* 7 (1), 21 art.
- Webb, P.W., 1975. Hydrodynamics and energetics of fish propulsion. *Bull. Fish. Res.* 190, 1–30.
- Wirsing, A.J., Heithaus, M.R., 2012. Behavioural transition probabilities in dugongs change with habitat and predator presence: implications for sirenian conservation. *Mar. Freshwater Res.* 63, 1069–1076. <https://doi.org/10.1071/MF12074>.